# Enhanced Superconductivity in $Th_2Mo_2Ru_2Si_4C$ with a Collapsed Intergrowth Structure

Yun-Lei Sun(孙云蕾)[1,2†], Hua-Xun Li(李华旬)[2,3†*], Yi-Qiang Lin(林以强)[2], Liang-Wen Ji(吉良雯)[4], Chang-Chao Liu(刘长超)[2], Jia-Yi Lu(卢佳依)[2], Wen-Lei Li(李文蕾)[2], Yi Liu(刘艺)[2], Hao Jiang(蒋好)[5], Ji-Yong Liu(刘继永)[6], Yunhao Lu(陆赟豪)[2], Yuke Li(李玉科)[3], and Guang-Han Cao(曹光旱)[2,7,8*]

[1]*Key Laboratory of Quantum Materials Control of Zhejiang Province, School of Information and Electrical Engineering, Hangzhou City University, Hangzhou 310015, China*
[2]*School of Physics, Zhejiang University, Hangzhou 310058, China*
[3]*School of Physics, and Hangzhou Key Laboratory of Quantum Matters, Hangzhou Normal University, Hangzhou 311121, China*
[4]*College of Electronics and Information Engineering, South-Central Minzu University, Wuhan 430074, China*
[5]*School of Physics and Optoelectronics, Xiangtan University, Xiangtan 411105, China*
[6]*Department of Chemistry, Zhejiang University, Hangzhou 310058, China*
[7]*Institute of Fundamental and Transdisciplinary Research, and State Key Laboratory of Silicon and Advanced Semiconductor Materials, Zhejiang University, Hangzhou 310058, China*
[8]*Collaborative Innovation Centre of Advanced Microstructures, Nanjing University, Nanjing 210093, China*

(Received 25 December 2025; accepted manuscript online 4 February 2026)

We report the discovery of bulk superconductivity in a new quinary intermetallic compound $Th_2Mo_2Ru_2Si_4C$, crystallized in a collapsed 22241-type structure. This structure is characterized by the intergrowth of $ThMo_2Si_2C$ and $ThRu_2Si_2$ units interconnected by equivalent Si-Si bonds that enhance inter-sublattice coupling. The refined lattice parameters are $a = 4.2212(1)$ Å and $c = 20.3899(7)$ Å. Electrical resistivity and magnetic susceptibility measurements of both polycrystalline and single-crystal samples consistently demonstrate bulk superconductivity with a transition temperature $T_c \sim 6.0$ K significantly higher than those of the constituent compound $ThMo_2Si_2C$ and its related analogs. Under magnetic fields, the superconducting state exhibits a nearly isotropic behavior, which is attributed to strong covalent interlayer coupling. First-principles calculations reveal a substantial contribution from the Mo-d orbitals near the Fermi level, which exhibit several band-crossing points. The enhancement in $T_c$ can be attributed to the synergistic combination of the valence electron concentration and the inter-sublattice self-doping effect between the $[Ru_2Si_2]$ and $[Mo_2Si_2C]$ layers.

DOI: 10.1088/0256-307X/43/3/030715 CSTR: 32039.14.0256-307X.43.3.030715

*1. Introduction.* Superconductivity can be induced or enhanced through various approaches such as chemical doping and the application of physical pressure to parent compounds.[1–10] A promising route for discovering new superconducting materials is to design intergrowth structures based on known superconducting building blocks.[11,12] This strategy facilitates the exploration of novel compounds as well as often induces a self-doping effect within the intergrown architecture that can intrinsically promote superconducting properties.[13] A representative example is the Fe-based superconductor $Ba_2Ti_2Fe_2As_4O$, adopting a 22241-type structure.[14,15] This structure can be interpreted as the intergrowth of the parent iron-based superconductor $BaFe_2As_2$ (with a $ThCr_2Si_2$ structure containing only anti-fluorite-type $[Fe_2As_2]$ layers)[16] and $BaTi_2As_2O$ (with a $CeCr_2Si_2C$ structure).[17,18] Charge transfer between the $[Fe_2As_2]$ and $[Ti_2As_2O]$ layers results in the coexistence of intrinsic bulk superconductivity and suppressed charge-density wave instability.[19]

The $ThCr_2Si_2$ structure comprises alternating layers of metal cations and antifluorite-type units.[20] In addition to compounds such as $BaFe_2As_2$, a class of *collapsed* phases (in which, the ratio of the lattice parameters satisfies $c/a < 2.58$) exists.[21,22] The $CaBe_2Ge_2$ structure is closely related to the $ThCr_2Si_2$ structure, which consists of alternating metal cations, fluorite-type layers, and antifluorite-type layers.[23] Because of their structural similarity and comparable formation energies, many compounds exhibit polymorphs, such as $ThM_2Si_2$ ($M$ is a transition metal).[24–27] By contrast, $ThMo_2Si_2C$, a recently discovered superconducting topological metal,[28,29] crystallizes in the $CeCr_2Si_2C$ structure. Inspired by the example of $Ba_2Ti_2Fe_2As_4O$, we recently extended the

†These authors contributed equally to this work.
*Corresponding authors. Email: lihuaxun@zju.edu.cn; ghcao@zju.edu.cn
© 2026 Chinese Physical Society and IOP Publishing Ltd. All rights, including for text and data mining, AI training, and similar technologies, are reserved.

22241-type structure to its collapsed variants, leading to the identification of two new structure types, denoted by 22241′ and 22241*. Specifically, the 22241′-type structure is formed by the alternating stacking of fluorite-type and $CeCr_2Si_2C$-type layers. The fluorite-type $[Si_2Ir_2]$ layer in $ThIr_2Si_2$ [30] can intergrow with $ThMo_2Si_2C$ to form the 22241′-type compound $Th_2Mo_2Ir_2Si_4C$, which exhibits a two-gap superconductivity behavior with $T_c$ = 3.4 K. [31] The 22241*-type structure consists of alternating fluorite-type, $CeCr_2Si_2C$-type, and antifluorite-type layers. This configuration is identified in $Th_2Mo_2Rh_2Si_4C$, where fluorite-type $[Si_2Rh_2]$ and antifluorite-type $[Rh_2Si_2]$ layers [32] intergrow with $ThMo_2Si_2C$. $Th_2Mo_2Rh_2Si_4C$ exhibits superconductivity with $T_c$ = 2.1 K. Interestingly, owing to the locally noncentrosymmetric structure, the electronic bands show splitting caused by Rashba-type spin-orbit coupling. [33]

Building on these findings and guided by lattice-matching analysis and formation energy calculations, In this study, we aimed to discover a newly collapsed 22241-type compound. Motivated by the critical roles of self-doping effects and valence electron concentration [34] in enhancing the superconductivity, we proposed replacing Rh and Ir with elements from other groups to achieve a higher superconducting transition temperature. Herein, we report the synthesis, crystal structure, and superconducting properties of a quinary intermetallic compound, $Th_2Mo_2Ru_2Si_4C$. A crystallographic analysis was performed to confirm the target structure, which can be described as an intergrowth of $ThMo_2Si_2C$ and $ThRu_2Si_2$ [35–37] (with a $ThCr_2Si_2$ structure), as illustrated in Fig. 1(a). Magnetic susceptibility and electrical resistivity measurements of both the polycrystalline and single-crystal samples, synthesized using the arc-melting method, demonstrate isotropic bulk superconductivity with $T_c \sim$ 6 K. This value is notably higher than that of the constituent compound $ThMo_2Si_2C$. In addition, band structure calculations suggest the presence of nontrivial topological states in this compound, motivating further investigations of its topological characteristics.

*2. Experimental.* $Th_2Mo_2Ru_2Si_4C$ was synthesized using the arc-melting method, with high-purity starting materials: Th (99.5%), Mo (99.9%), Ru (99.99%), Si (99.99%), and C (99.95%). First, the starting materials were weighed accurately in stoichiometric ratios and thoroughly mixed in a glovebox with water and oxygen content below 1 ppm. The mixture was subsequently pressed into a pellet and melted in an arc-melting furnace equipped with a water-cooled Cu hearth. An ingot of the target compound was obtained after several cycles of flipping and re-melting. Single-crystal samples were selected from the ingot (typical size of $\sim 1.0 \times 0.8 \times 0.03\,mm^3$ as shown in the inset of Fig. 1(c)). The remainder of the ingot was used as a polycrystalline sample for property measurements.

Powder X-ray diffraction (XRD) was performed at room temperature using a PANalytical diffractometer (Empyrean Series 2) equipped with Cu-$K_{\alpha 1}$ radiation source. The crystal structure was refined using Rietveld analysis. [38] Single-crystal XRD was performed using a Bruker D8 Venture diffractometer with Mo-$K_\alpha$ radiation. The chemical compositions of the single crystals were determined by energy-dispersive X-ray spectroscopy (EDS) using a field-emission scanning electron microscope (SEM; Hitachi S-3400N) equipped with an Oxford Instruments X-Max spectrometer. A Quantum Design Magnetic Property Measurement System (MPMS3) was used to measure the magnetization of the samples. Electrical resistivity and specific heat were measured using a Quantum Design Physical Property Measurement System (PPMS-9, Dynacool).

First-principles calculations were performed within the generalized gradient approximation (GGA) by using the Vienna Ab-initio Simulation package (VASP). The experimental crystal structure parameters were used for the initial relaxation. The forces were minimized to less than 0.0001 eV/Å during relaxation. A plane-wave basis energy cutoff of 500 eV was employed alongside a $12 \times 12 \times 2$ $\Gamma$-centered $k$-point mesh for density of states calculations.

*3. Results and Discussion.* The 22241-type intergrowth structure of $Th_2Mo_2Ru_2Si_4C$ is illustrated schematically in Fig. 1(a). The constituent compounds $ThMo_2Si_2C$ and $ThRu_2Si_2$ adopted the $CeCr_2Si_2C$-type and collapsed $ThCr_2Si_2$-type structures, respectively. The cell parameter $a$ axis of $ThRu_2Si_2$ is $a_{122}$ = 4.188 Å, [37] while that of $ThMo_2Si_2C$ is $a_{1221}$ = 4.2296 Å. [28] Thus, the lattice mismatch between them is $\mu = 2|a_{1221} - a_{122}|/(a_{1221} + a_{122}) = 0.99\%$. By employing an empirical block-layer model, [12] we designed the 22241-type structure by alternatingly stacking $[Mo_2Si_2C]$ and $[Ru_2Si_2]$ layers. Notably, the $[Mo_2Si_2C]$ and $[Ru_2Si_2]$ sublattices are interconnected via equivalent Si-Si bonds, as indicated in Fig. 1(b).

Compositional analysis of the single crystals was performed using EDS. The measured atomic ratios were Th : Mo : Ru : Si=1.95(9) : 1.96(11) : 2.00(11) : 4.45(24) (Fig. 1(c)), consistent with the nominal stoichiometry of $Th_2Mo_2Ru_2Si_4C$ within measurement uncertainty. Although the carbon content could not be quantified because of the detection limitations of EDS for light elements, The reasonable agreement between the refined and expected compositions within experimental error supports the proposed formula.

Further structural validation was performed using single-crystal XRD. The reconstructed ($hk0$) and ($0kl$) reciprocal lattice planes are shown in Fig. 1(d). The ($h0l$) plane is provided in Fig. S1(a) of the Supplementary Material (SM) for completeness. The presence of ($01l$) diffraction spots exclusively within the green rectangle for $l$ = odd numbers in Fig. 1(e) is characteristic of body-centered lattice symmetry. During the structural refinement, the atomic occupancy parameters were allowed to vary freely. The refinement results (Table S1 in the SM) show that all atomic sites are close to full occupancy, with the exception of site C, which exhibited a slight deficiency (occupancy ∼0.93(5)). Note that this value carries a relatively large uncertainty because XRD is less sensitive to light-element carbon. Thus, precisely quantifying the amount of C vacancies is challenging. The possibility of site mixing between Mo and Ru was evaluated using refinement models allowing for mutual occupancy were tested; however,

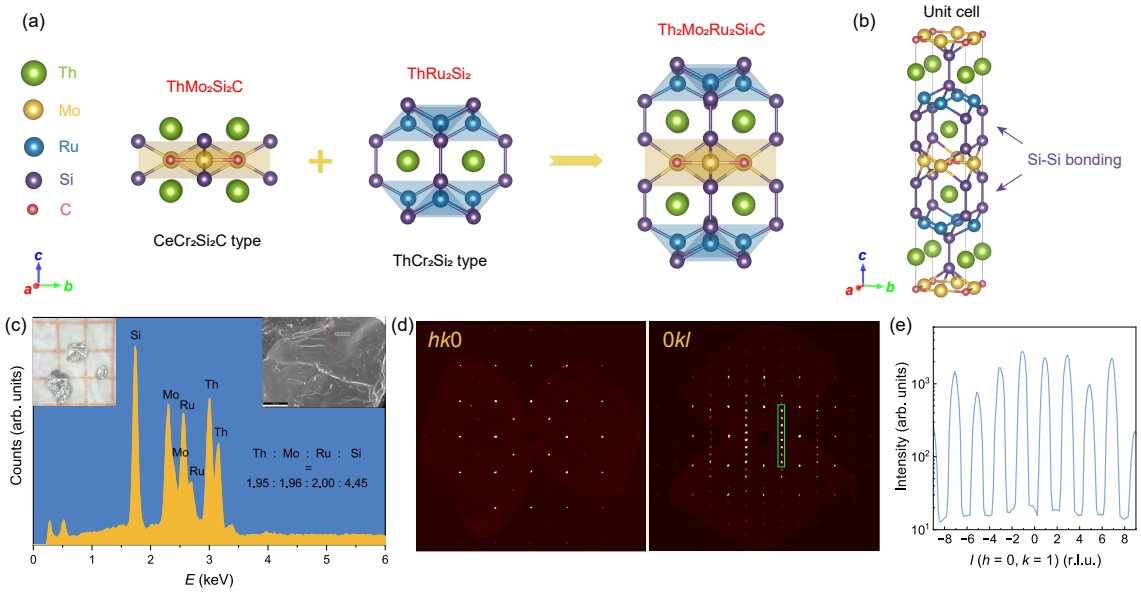


**Fig. 1.** (a) Schematic of the crystal structure of $Th_2Mo_2Ru_2Si_4C$, resulting from the intergrowth of $ThMo_2Si_2C$ and $ThRu_2Si_2$ units along the crystallographic $c$-axis. (b) The unit cell of $Th_2Mo_2Ru_2Si_4C$. The interlayer Si-Si bonds are indicated by arrows. (c) EDS spectrum of the single crystals. (d) Reconstructed ($hk0$) and ($0kl$) reciprocal lattice planes obtained from single-crystal XRD data. (e) Intensity profile of the diffraction spots corresponding to the diffraction planes with Miller indices ($01l$) extracted from the green rectangle in panel (d).

**Table 1.** The crystallographic data of $Th_2Mo_2Ru_2Si_4C$ with the 22241 structure obtained from the room-temperature single-crystal XRD.

| | |
|---|---|
| Chemical formula | $Th_2Mo_2Ru_2Si_4C$ |
| Formula weight | 982.47 g/mol |
| X-ray wavelength | 0.71073 Å |
| Crystal system | Tetragonal |
| Space group | $I4/mmm$ |
| Unit-cell dimensions | $a = 4.2212(1)$ Å, $\alpha = 90°$<br>$b = 4.2212(1)$ Å, $\beta = 90°$<br>$c = 20.3899(7)$ Å, $\gamma = 90°$ |
| Volume | 363.32(2) Å$^3$ |
| $Z$ | 2 |
| Density (calculated) | 8.981 g/cm$^3$ |
| $F(000)$ | 828 |
| Crystal size | $0.04 \times 0.04 \times 0.02$ mm$^3$ |
| $\theta$ range for data collection | 7.996° to 56.672° |
| Index ranges | $-5 \le h \le 5$, $-5 \le k \le 5$, $-26 \le l \le 26$ |
| Reflections collected | 6866 |
| Independent reflections | 168 [$R_{int} = 0.0302$] |
| Data/restraints/parameters | 168/0/18 |
| Goodness-of-fit | 1.024 |
| Final $R^*$ indices [$I \le 2\sigma(I)$] | $R_{obs} = 0.0089$, $wR_{obs} = 0.0185$ |
| $R^*$ indices [all data] | $R_{all} = 0.0089$, $wR_{all} = 0.0185$ |
| Largest diff. peak and hole | 0.51 and $-0.95$ e·Å$^{-3}$ |

| Atom | $x$ | $y$ | $z$ | Occupancy | $U_{(eq)}$ | $U_{11}$ | $U_{22}$ | $U_{33}$ | $U_{12}$ | $U_{13}$ | $U_{23}$ |
|---|---|---|---|---|---|---|---|---|---|---|---|
| Th | 0 | 0 | 0.63063(2) | 1 | 6.1(1) | 6.6(1) | 6.6(1) | 5.0(1) | 0 | 0 | 0 |
| Ru | 0.5 | 0 | 0.75 | 1 | 5.1(1) | 5.1(2) | 5.1(2) | 4.9(2) | 0 | 0 | 0 |
| Mo | 0 | 0.5 | 0.5 | 1 | 5.3(1) | 4.8(3) | 6.0(3) | 4.9(2) | 0 | 0 | 0 |
| Si(1) | 0.5 | 0.5 | 0.57390(9) | 1 | 7.2(4) | 7.4(5) | 7.4(5) | 6.9(9) | 0 | 0 | 0 |
| Si(2) | 0.5 | 0.5 | 0.69499(9) | 1 | 5.5(3) | 6.5(5) | 6.5(5) | 3.5(8) | 0 | 0 | 0 |
| C | 0 | 0 | 0.5 | 1 | 12(2) | 11(3) | 11(3) | 15(5) | 0 | 0 | 0 |

they did not lead to better agreement with the experimental data. To further assess the site preference, we computed the formation energies of the two structural models: fully ordered $Th_2Mo_2Ru_2Si_4C$ and a configuration with swapped Mo/Ru sites ($Th_2Ru_2Mo_2Si_4C$). The swapped configuration was found to be energetically less favorable by approximately 2.83 eV per formula unit, This suggests a thermodynamically stable ordered arrangement. Based on these observations, the final refinement was performed by fixing at 1 for all atomic sites, as shown in Table 1. The structural parameters show excellent consistency with those from powder XRD refinement of

polycrystalline samples (see below), providing conclusive evidence of the successful synthesis of the 22241-type structure in $Th_2Mo_2Ru_2Si_4C$. Notably, the bond length of the interlayer Si-Si bonding is 2.47 Å, similar to those of $ThRu_2Si_2$ [37] and $ThMo_2Si_2C$,[28] resulting in a collapsed 22241-type structure.

Rietveld refinement [38] of powder XRD on polycrystalline samples was performed to confirm the target 22241 structural model. In accordance with the results of the single-crystal refinement, the occupancies of all atomic sites were fixed at full occupation. As shown in Fig. S1(b) of the SM, the experimental pattern exhibits excellent agreement with the simulated one, with all major peaks indexed to the tetragonal space group $I4/mmm$ (No. 139). A few minor peaks were identified as impurities of $ThMo_2Si_2C$ and $ThO_2$ with weight fractions of 3.6% and 1.2%, respectively. Although these impurities reflect the challenge of the phase-pure synthesis of polycrystalline samples, their low concentrations do not compromise the identification of the dominant $Th_2Mo_2Ru_2Si_4C$ phase and the bulk nature of its superconductivity. The presence of reflections with Miller indices $(hkl)$, satisfying $h+k+l=$ even numbers, confirms the body-centered lattice symmetry. The refinement converged satisfactorily with a reliability factor $R_{wp} = 6.58\%$ and a goodness-of-fit index $S = 2.09$. The refined cell parameters are $a = 4.21817(4)$ Å and $c = 20.3684(2)$ Å (see Table S2 in the SM for full details). These results are consistent with those obtained from single-crystal refinement, further validating the designed structure.

Figure 2(a) shows the temperature-dependent electrical resistivity, measured with a current parallel to the $ab$ plane ($I \parallel ab$) for a $Th_2Mo_2Ru_2Si_4C$ single crystal in zero magnetic field. Upon cooling, the resistivity exhibits metallic behavior with a residual resistivity ratio (RRR) of ∼1.3. This implies that the sample is in the dirty limit owing to impurity scattering. This scattering could be attributed to possible C vacancies, as revealed by XRD analyses. A superconducting transition is observed with an onset temperature $T_c^{onset} = 6.44$ K, and a zero-resistance state is achieved at $T_c^{zero} = 5.79$ K. Notably, the transition temperature exhibited a three-fold enhancement over that of $ThMo_2Si_2C$,[28] which will be discussed in detail later. Similar metallic behavior, with RRR ∼1.41, is observed in the polycrystalline samples (see Figs. S2(a) and S2(b) in the SM). The room-temperature resistivity is approximately 1.6 mΩ·cm, which is comparable to that of $ThMo_2Si_2C$ [28] but two orders of magnitude larger than that of $ThRu_2Si_2$.[37] The broader superconducting transition observed in the polycrystalline samples is likely due to weak links at the grain boundaries and the microstructural inhomogeneity attributed to these impurity phases and possible C vacancies.

To examine the anisotropy of the superconducting properties, we performed magnetoresistance measurements on single crystals under external magnetic fields $H \parallel c$ and $H \perp c$. The corresponding in-plane resistivity curves are presented in Figs. 2(b) and 2(c), respectively. The superconducting transition is progressively suppressed to lower temperatures with increasing magnetic field. The upper critical field $H_{c2}(T)$ was determined from the temperature at which the resistivity reaches 90% of its normal-state value at 7 K. As shown in Figs. 2(d) and 2(e), the zero-temperature upper critical fields $\mu_0 H_{c2}(0)$ were estimated using the Ginzburg–Landau (GL) relation $H_{c2}(T) = H_{c2}(0)(1-t^2)/(1+t^2)$, where $t = T/T_c$. The obtained values are 4.91 T for $H \parallel c$ and 4.85 T for $H \perp c$. Therefore, the quantitative anisotropy is $H_{c2}^{\parallel c}(0)/H_{c2}^{\perp c}(0) \approx 1.01$.

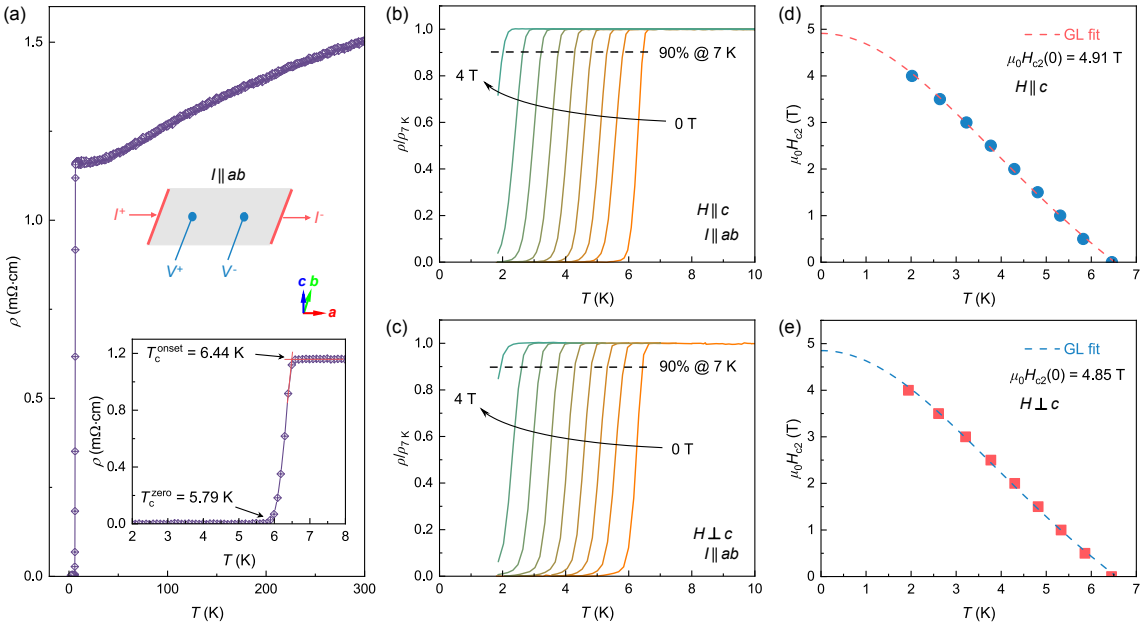


**Fig. 2.** (a) Temperature dependence of the in-plane electrical resistivity ($I \parallel ab$) for a $Th_2Mo_2Ru_2Si_4C$ single crystal under zero external magnetic field. (b) and (c) Temperature and field dependence of the in-plane normalized electrical resistivity with external magnetic fields $H \parallel c$ and $H \perp c$, respectively. (d) and (e) Upper critical fields $H_{c2}(T)$ extracted from the in-plane resistivity data for $H \parallel c$ and $H \perp c$, respectively.

Therefore, we do not distinguish between the in-plane and out-of-plane upper critical fields nor between the corresponding coherence lengths $\xi = \sqrt{\Phi_0/2\pi\mu_0 H_{c2}(0)} = 8.2\,\text{nm}$. This nearly isotropic behavior may be attributed to the strong inter-sublattice coupling mediated by covalent Si-Si bonding, despite the layered superlattice structure. Another important factor is that the sample resides within the dirty limit, where strong scattering from defects can reduce the electronic anisotropy by decreasing the electron mean free path, thereby lowering the coherence length.[39]

Figures 3(a) and 3(b) present the low-temperature dc magnetic susceptibility $\chi(T)$ of a single crystal measured under an applied field of 10 Oe oriented both parallel and perpendicular to the crystallographic $c$ axis in field-cooled (FC) and zero-field-cooled (ZFC) modes. A pronounced diamagnetic response emerged below 6 K, corroborating the superconducting transition identified in the electrical resistivity measurements. The magnetic shielding fraction approached 100% for $H \perp c$ at 1.8 K, confirming bulk superconductivity. For $H \parallel c$, the shielding fraction exceeds 100% owing to the demagnetization effect. Bulk superconductivity was also confirmed by the temperature dependence of the magnetic susceptibility of the polycrystalline samples, as shown in Fig. S2(c) of the SM.

Figures 3(c) and 3(d) show the magnetization curves $M(H)$ measured at various temperatures between 1.8 and 5.4 K for $H \parallel c$ and $H \perp c$, respectively. In the low-field regime, the $M$–$H$ relationship exhibits linear behavior, which we fit to the linear function $M_{\text{fit}}$ (represented by black dashed lines). The lower critical field $H_{c1}(T)$ is determined from the deviation of the magnetization from this linear fit:[40] using the criterion of $1\,\text{emu}\cdot\text{cm}^{-3}$ as the threshold for flux penetration. By subtracting $M_{\text{fit}}$ from the measured $M(H)$ data, we obtained the deviation in the magnetization. With corrections for the demagnetization effects, we applied this consistent criterion to determine $H_{c1}(T)$ for both field orientations, as shown in Figs. 3(e) and 3(f).

As shown, the temperature dependence of $H_{c1}(T)$ cannot be described by GL theory $H_{c1}(T) = H_{c1}(0)(1-t^2)$, where $t = T/T_c$. Therefore, we attempted to analyze the $H_{c1}(T)$ data using a single s-wave gap and two s-wave gap models. Within this framework, $H_{c1}(T)$ is correlated with the normalized superfluid density using the following relation:[41,42]

$$\frac{H_{c1}(T)}{H_{c1}(0)} = \rho_s = 1 + 2\int_{\Delta}^{\infty} dE \frac{\partial f}{\partial E} \frac{E}{\sqrt{E^2 - \Delta(t)^2}},$$

where $f(E)$ denotes the Fermi function and $t = T/T_c$ represents the reduced temperature. The temperature dependence of the BCS-like gap $\Delta(t)$ can be approximated as: $\Delta(t) = \Delta_0 \tanh\{1.82[1.018(1/t-1)]^{0.51}\}$. In the two-gap scenario, the total superfluid density is considered as the weighted sum: $\rho_s = w\rho_s(\Delta_1) + (1-w)\rho_s(\Delta_2)$.

The single-gap model reproduced the experimental data well. However, from the perspective of band structure, the material may be a multiband system. Therefore, we conducted a two-gap analysis. Consequently, the two-gap model provided a good fit and yielded the following parameters: For $H \parallel c$, $\Delta_1^{\parallel c}(0) = 0.59 k_B T_c$, $\Delta_2^{\parallel c}(0) = 0.59 k_B T_c$, $w = 0.56$, and $H_{c1}^{\parallel c}(0) = 17.4\,\text{Oe}$. For $H \perp c$, $\Delta_1^{\parallel c}(0) = 0.49 k_B T_c$, $\Delta_2^{\parallel c}(0) = 0.55 k_B T_c$, $w = 0.55$, and $H_{c1}^{\perp c}(0) = 19.6\,\text{Oe}$. The negligible anisotropy in $H_{c1}(0)$ is consistent with the observed isotropic behavior of $H_{c2}(0)$,

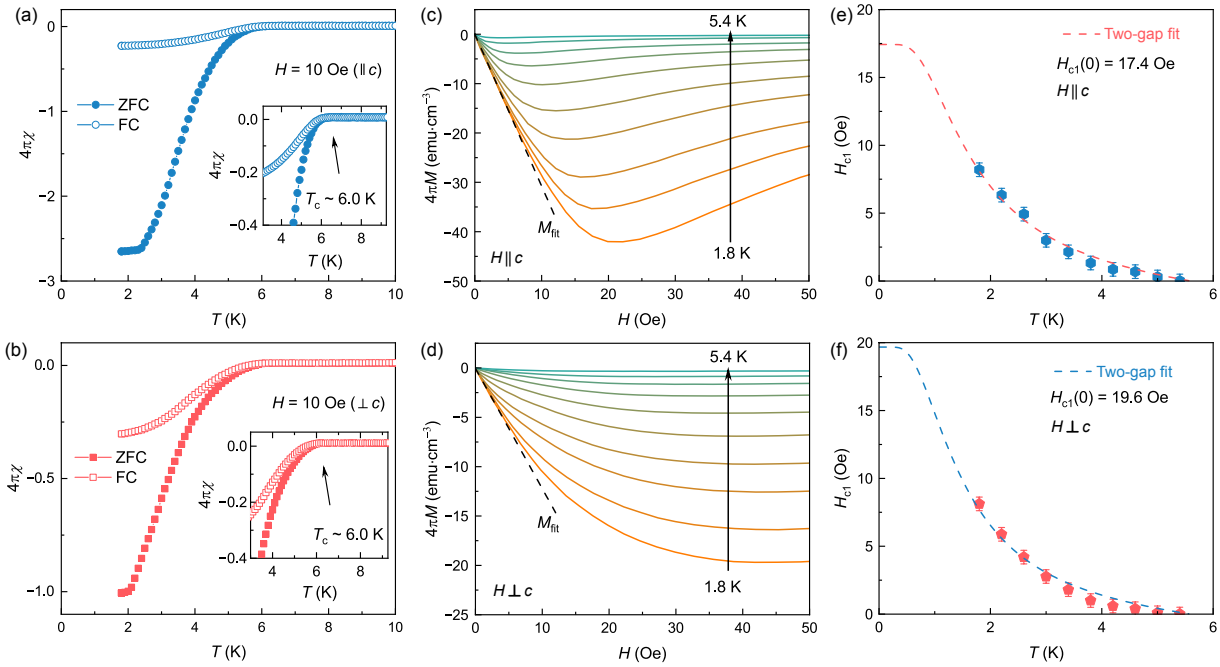


**Fig. 3.** (a) and (b) Temperature dependence of the magnetic susceptibility for a $Th_2Mo_2Ru_2Si_4C$ single crystal under an applied magnetic field of $H = 10\,\text{Oe}$ ($H \parallel c$ and $H \perp c$). (c) and (d) Magnetization as a function of the external field at different temperatures for both $H \parallel c$ and $H \perp c$ orientations. The dashed lines represent linear fittings in the low-field region. (e) and (f) Determined values of the lower critical fields $H_{c1}$ for both $H \parallel c$ and $H \perp c$ directions.

further supporting the picture of nearly isotropic superconducting properties of this material. Subsequently, a penetration depth $\lambda = 620\,\text{nm}$ can be derived from $\mu_0 H_{c1}(0) = \ln(\lambda/\xi)\Phi_0/(4\pi\lambda^2)$. The resulting Ginzburg–Landau parameter $\kappa = \lambda/\xi = 76$ indicates that the $Th_2Mo_2Ru_2Si_4C$ is a type-II superconductor.

Because of the insufficient size and quantity of single crystals for specific heat measurements, data were collected from polycrystalline $Th_2Mo_2Ru_2Si_4C$. Figure 4 shows the temperature dependence of the specific heat measured in zero magnetic field. The data are displayed as $C/T$ versus $T^2$ between 1.8 and 8 K. Above the superconducting transition, the data exhibited a linear trend, which arises from the combination of an electronic term ($\propto T$) and a phonon term ($\propto T^3$). Normal-state data below 8 K were fitted using the expression $C/T = \gamma + \beta T^2$: from which we obtained the Sommerfeld coefficient $\gamma = 21.5\,\text{mJ}\cdot\text{mol}^{-1}\cdot\text{K}^{-2}$ and phonon coefficient $\beta = 0.26\,\text{mJ}\cdot\text{mol}^{-1}\cdot\text{K}^{-4}$. The Debye temperature was estimated from $\beta$ using the relation $\Theta_D = [(12\pi^4 NR)/(5\beta)]^{1/3}$, and found to be $\Theta_D = 434\,\text{K}$, where $N$ denotes the number of atoms per formula unit and $R$ is the gas constant.

A pronounced but broad jump in the specific heat is observed below $T_c \sim 5.8\,\text{K}$, indicating the onset of bulk superconductivity, which is consistent with the results obtained from electrical transport and magnetic measurements (Fig. S2 in the SM). The electronic contribution to the specific heat in the superconducting state was isolated by subtracting the phonon contribution as $C_e = C - \beta T^3$. The resulting normalized electronic specific heat $C_e/\gamma T$ are shown in the inset of Fig. 4. The broad superconducting transition cannot be adequately described using a single modified BCS model,[43] likely because of a combination of factors. In addition to possible inhomogeneities in the polycrystalline samples that smear the transition, two-gap behavior with similar superconducting gaps $\Delta_1$ and $\Delta_2$ indicated by the $H_{c1}(T)$ analysis,

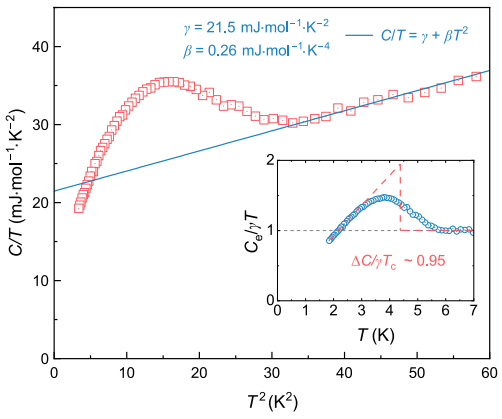


**Fig. 4.** Low-temperature specific heat for polycrystalline samples of $Th_2Mo_2Ru_2Si_4C$, presented as $C/T$ versus $T^2$. The blue line represents a linear fit of the normal-state data to $C/T = \gamma + \beta T^2$. The inset shows the normalized electronic specific heat $C_e/\gamma T$ obtained by subtracting the phonon contribution. Dashed red lines mark the jump during the superconducting transition.

causes the individual specific heat jumps associated with each gap to merge into a single broader anomaly. We attempted to decompose electronic specific heat using a two-gap model. However, the extracted fitting parameters such as the individual gap size and weight are highly uncertain and not convincing for a quantitative conclusion. Given the current data quality, a more in-depth analysis is not feasible for obtaining definitive gap information.

To estimate the specific heat jump near $T_c$, we linearly extrapolated the low-temperature data to higher temperatures, while enforcing entropy conservation around the transition. This procedure yielded a normalized specific heat jump of $\Delta C/\gamma T_c \sim 0.95$, which is lower than the weak-coupling BCS value of 1.43.[44] This reduction implies a smaller superconducting gap compared with the weak-coupling BCS expectation $\Delta_0^{BCS} = 1.76 k_B T_c = 0.9\,\text{meV}$, Additionally, the resistivity measurements [Fig. 2(a)] indicate that the sample lies within the dirty limit, characterized by short mean electron-free paths. In such materials, the enhanced scattering from impurities, defects, or grain boundaries can further broaden the superconducting transition and suppress the specific heat jump.

Finally, we performed first-principles calculations on $Th_2Mo_2Ru_2Si_4C$ to elucidate its electronic structure. Figure 5(a) shows the electronic band structure projected onto the Mo-d and Ru-d orbitals, along with the total and atom-projected densities of the states (DOS) near the Fermi energy including contributions from the Th-d, Mo-d, Ru-d, Si-p, and C-p orbitals. Electronic structure calculations showed a significant contribution of delocalized valence electrons to the total DOS characteristics of intermetallic compounds. Projection analysis shows that the Mo-d orbitals dominate the DOS at the Fermi level ($E_F$), whereas the Ru-d orbitals provided a secondary contribution. The computed total DOS at $E_F$ is $N(E_F) = 5.6\,\text{eV}^{-1}\cdot\text{f.u.}^{-1}$, which corresponds to the bare Sommerfeld coefficient, $\gamma_{bare} = \frac{1}{3}\pi^2 k_B^2 N(E_F) = 15.50\,\text{mJ}\cdot\text{mol}^{-1}\cdot\text{K}^{-2}$. When the electron–phonon coupling strength ($\lambda_{ph}$, provided in Table 2) is considered using the relation $\gamma_{th} = \gamma_{bare}(1+\lambda_{ph})$, the theoretical value was comparable to the experimental value.

The calculated band structure reveals multiple bands crossing the Fermi level, suggesting that $Th_2Mo_2Ru_2Si_4C$ is a multi-band superconductor. Thus, the experimentally observed two-gap behavior may have originated from its multiband nature. Notably, several band-crossing points are identified near the Fermi level (marked with magenta arrows) originate primarily from the Mo-d orbitals. Previous theoretical studies suggested $ThMo_2Si_2C$ is a potential topological Dirac metal,[29] $Th_2Mo_2Ru_2Si_4C$ may also have a nontrivial band topology. Further detailed investigations such as topological invariant analysis is valuable for fully covering topological characteristics.

To evaluate the interlayer coupling quantitatively, we performed a crystal orbital Hamilton population (COHP) analysis on the inter-sublattice Si-Si bonds, as indicated by the arrows in Fig. 1(b). As shown in Fig. 5(b), the COHP curve exhibits pronounced negative peaks deep below the

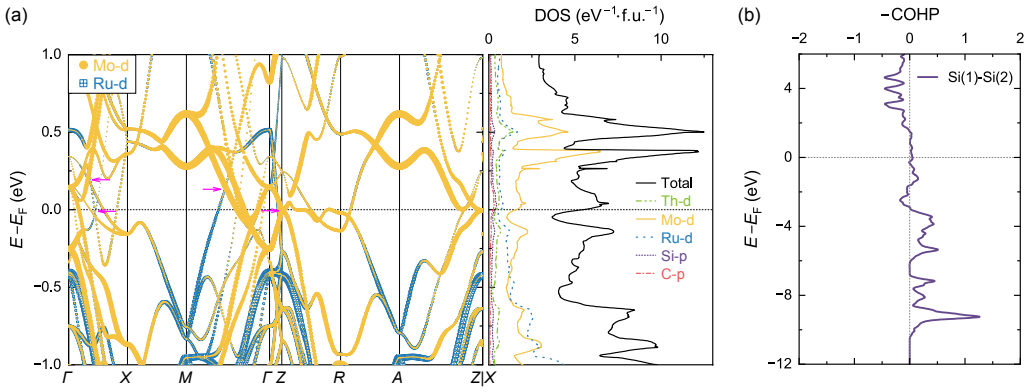


**Fig. 5.** (a) Electronic band structure projected on Mo-d and Ru-d orbitals, and density of states with contributions from Th-d, Mo-d, Ru-d, Si-p, and C-p orbitals around the Fermi energy for $Th_2Mo_2Ru_2Si_4C$. Magenta arrows indicate multiple band-crossing points. (b) COHP analyses of inter-sublattice Si-Si bonding, as indicated by the arrows in Fig. 1(b).

**Table 2.** Superconducting and normal-state parameters of $ThMo_2Si_2C$, $Th_2Mo_2Ru_2Si_4C$, $Th_2Mo_2Rh_2Si_4C$, and $Th_2Mo_2Ir_2Si_4C$. The electron–phonon coupling strength $\lambda_{ph}$ is estimated by using the McMillan formula.[45] VEA denotes valance electrons per atom.

| Parameters | $ThMo_2Si_2C$[28] | $Th_2Mo_2Ru_2Si_4C$ [this work] | $Th_2Mo_2Rh_2Si_4C$[33] | $Th_2Mo_2Ir_2Si_4C$[31] |
|---|---|---|---|---|
| $T_c$ (K) | 2.2 | 6.0 | 2.1 | 3.4 |
| $H_{c2}(0)$ (kOe) | 2.66 | 48.8 | 13.9 | 9.50 |
| $H_{c1}(0)$ (Oe) | 16 | 18.5 | 34 | 38 |
| $\Delta C/\gamma_n T_c$ | 0.98 | 0.95 | 1.39 | 1.00 |
| $\xi$ (nm) | 35.2 | 8.2 | 15.4 | 18.6 |
| $\lambda$ (nm) | 528 | 620 | 385 | 358 |
| $\kappa$ | 15 | 76 | 25 | 19 |
| $\lambda_{ph}$ | 0.49 | 0.61 | 0.54 | 0.60 |
| $\gamma$ (mJ·mol$^{-1}$·K$^{-2}$) | 11.4 | 21.5 | 17.90 | 20.77 |
| $\Theta_D$ (K) | 351 | 434 | 235 | 245 |
| VEA | 4.67 | 5.09 | 5.27 | 5.27 |

Fermi level confirm the formation of stable bonding states. The integrated COHP (ICOHP) value up to the Fermi level is −1.87230 eV, which signifies a substantial covalent bonding strength for the Si-Si interaction. This electronic structure analysis provides compelling evidence of strong inter-sublattice coupling mediated by covalent Si-Si bonds.

The superconducting parameters of $Th_2Mo_2Ru_2Si_4C$ are summarized in Table 2, in comparison with those of $ThMo_2Si_2C$,[28] $Th_2Mo_2Rh_2Si_4C$,[33] and $Th_2Mo_2Ir_2Si_4C$.[31] A notable finding is the significant enhancement in the superconducting transition temperature $T_c$ of $Th_2Mo_2Ru_2Si_4C$, which is nearly three times higher than that of $ThMo_2Si_2C$. This pronounced increase may be attributed to two factors. First, in intermetallic or alloys superconductors, empirical rules often connect superconducting transition temperatures with the number of valence electrons per atom. Previous studies have suggested that the optimal conditions for superconductivity occur at approximately 5 and 7 valence electrons per atom.[34] $Th_2Mo_2Ru_2Si_4C$, with a valence electron count closer to 5 (Fig. S4(b) in the SM), satisfies this criterion more effectively compared to other compounds, thereby supporting a higher $T_c$. In addition, we compared the DOS at the Fermi level as a function of the valence electron count for $Th_2Mo_2Ru_2Si_4C$, $Th_2Mo_2Rh_2Si_4C$, $Th_2Mo_2Ir_2Si_4C$, and $ThMo_2Si_2C$, as shown in Fig. S3(a) of the SM. The calculated $N(E_F)$ for $Th_2Mo_2Ru_2Si_4C$ is not the largest among this series, although it exhibits the highest $T_c$. Therefore, the $T_c$ enhancement is likely the result of multiple factors and requires further investigations. Second, electronic structure considerations provide additional insights. Compared to $Th_2Mo_2Rh_2Si_4C$[33] and $Th_2Mo_2Ir_2Si_4C$,[31] the Fermi level in $Th_2Mo_2Ru_2Si_4C$ shifts upward relative to the Mo-d orbital-dominated bands. This suggests a more substantial self-doping effect, whereby electrons are effectively transferred from the $[Ru_2Si_2]$ layer to the $[Mo_2Si_2C]$ layer. To quantitatively verify the proposed self-doping effect, we conducted a Bader charge analysis (results summarized in Table S3 of the SM). The analysis reveals that the Bader charge on the $[Mo_2Si_2C]$ block is 0.0875 times greater than that of the $[Ru_2Si_2]$ block, confirming charge transfer from the $[Ru_2Si_2]$ layer to the $[Mo_2Si_2C]$ layer in $Th_2Mo_2Ru_2Si_4C$. Such charge redistribution likely strengthens the interlayer coupling and contributes to the increase in $T_c$. These two effects–valence-electron concentration and layer-dependent self-doping–may work synergistically to enhance the superconductivity of $Th_2Mo_2Ru_2Si_4C$. Further theoretical and experimental studies are needed to quantitatively evaluate the proposed mechanisms and uncover other possible contributing factors.

The significantly enhanced upper critical field observed in $Th_2Mo_2Ru_2Si_4C$ compared to $ThMo_2Si_2C$, $Th_2Mo_2Rh_2Si_4C$, and $Th_2Mo_2Ir_2Si_4C$, can be attributed to several interconnected factors in addition to a higher $T_c$. The first is the substantially reduced coherence length of $\xi = 8.2\,\text{nm}$. According to the standard relation $H_{c2}(0) = \Phi_0/2\pi\xi^2$, a shorter coherence length directly leads to an increase $H_{c2}$. This reduction in $\xi$ likely stems from disorder effects[46] induced by vacancies at the C sites, as evidenced by single-crystal XRD refinement. In addition, the electron–phonon coupling strength $\lambda_{ph} = 0.61$ is the highest among the four compounds. Stronger electron–phonon interactions may result in a larger effective quasiparticle mass and enhanced pair breaking under magnetic fields,[47] both of which could further increase the upper critical field. These two mechanisms, shorter coherence length and stronger electron–phonon coupling, collectively enhanced $H_{c2}(0)$ in the $Th_2Mo_2Ru_2Si_4C$.

*4. Conclusion.* We synthesized a new quinary compound, $Th_2Mo_2Ru_2Si_4C$, in both polycrystalline and single-crystalline forms, using the arc-melting method. Electrical and magnetic measurements revealed isotropic superconducting properties with an enhanced transition temperature $T_c \sim 6.0\,\text{K}$, and a relatively high upper critical field of $\mu_0 H_{c2} = 4.88\,\text{T}$. The enhanced superconductivity can be attributed to the valence electron concentration and self-doping effect between the $[Ru_2Si_2]$ and $[Mo_2Si_2C]$ layers. Furthermore, the material exhibited features suggestive of nontrivial band topology. This makes it a candidate material for exploring the interplay between superconductivity and topological states; its topological nature should be confirmed in future studies.

*Acknowledgements.* This work was supported by the National Key Research and Development Program of China (Grant Nos. 2022YFA1403202 and 2023YFA1406101) and the CAS Superconducting Research Project (Grant No. SCZX-0101). We thank Prof. Qing-Hu Chen for the helpful discussions.

# References

[1] Kamihara Y, Watanabe T, Hirano M, and Hosono H 2008 *J. Am. Chem. Soc.* **130** 3296
[2] Armitage N P, Fournier P, and Greene R L 2010 *Rev. Mod. Phys.* **82** 2421
[3] Sun H, Huo M, Hu X, Li J, Liu Z, Han Y, Tang L, Mao Z, Yang P, Wang B, Cheng J, Yao D X, Zhang G M, and Wang M 2023 *Nature* **621** 493
[4] Flores-Livas J A, Boeri L, Sanna A, Profeta G, Arita R, and Eremets M 2020 *Phys. Rep.* **856** 1
[5] Lee P A, Nagaosa N, and Wen X G 2006 *Rev. Mod. Phys.* **78** 17
[6] Guo J, Wu Q, and Sun L L 2018 *Acta Phys. Sin.* **67** 207409 (in Chinese)
[7] Huang Q, Zhao J, Lynn J W, Chen G F, Luo J L, Wang N L, and Dai P 2008 *Phys. Rev. B* **78** 054529
[8] Zhang K, Guo J, Wang Y, Wu X, Huang X, and Cui T 2025 *Chin. Phys. Lett.* **42** 110704
[9] Chen G F, Li Z, Li G, He W Z, Dong J, Zhang J, Zhang X D, Zhou P, Wang N L, and Luo J L 2008 *Chin. Phys. Lett.* **25** 3403
[10] Nie J Y, Yang X F, Chen K Y, Liu X Q, Xia W, Wang J, Zhang R, Dai D Z, Zhao C C, Tu C P, Dong H L, Jin X B, Deng J K, Zhang X, Guo Y F, and Li S Y 2025 *Chin. Phys. Lett.* **42** 070713
[11] Martin C, Maignan A, Huve M, Hervieu M, Michel C, and Raveau B 1991 *Physica C* **79** 1
[12] Wang Z C, Wu S Q, Ji L W, and Cao G H 2021 *Nano Res.* **14** 3629
[13] Wang Z C and Cao G H 2018 *Acta Phys. Sin.* **67** 207406 (in Chinese)
[14] Sun Y L, Jiang H, Zhai H F, Bao J K, Jiao W H, Tao Q, Shen C Y, Zeng Y W, Xu Z A, and Cao G H 2012 *J. Am. Chem. Soc.* **134** 12893
[15] Ablimit A, Sun Y L, Jiang H, Bao J K, Zhai H F, Tang Z T, Liu Y, Wang Z C, Feng C M, and Cao G H 2017 *J. Alloys Compd.* **694** 1149
[16] Rotter M, Tegel M, and Johrendt D 2008 *Phys. Rev. Lett.* **101** 107006
[17] Wang X F, Yan Y J, Ying J J, Li Q J, Zhang M, Xu N, and Chen X H 2010 *J. Phys.: Condens. Matter* **22** 075702
[18] Kelly N D 2025 *Solid State Sci.* **169** 108085
[19] Sun Y L, Ablimit A, Bao J K, Jiang H, Zhou J, and Cao G H 2013 *Sci. Technol. Adv. Mater.* **14** 055008
[20] Shatruk M 2019 *J. Solid State Chem.* **272** 198
[21] Jia S, Williams A J, Stephens P W, and Cava R J 2009 *Phys. Rev. B* **80** 165107
[22] Reehuis M and Jeitschko W 1990 *J. Phys. Chem. Solids* **51** 961
[23] Parthé E, Chabot B, Braun H F, and Engel N 1983 *Acta Cryst. B* **39** 588
[24] Shelton R N, Braun H F, and Musick E 1984 *Solid State Commun.* **52** 797
[25] Hiebl K and Rogl P F 1987 *J. Nucl. Mater.* **144** 193
[26] Buffat B, Chevalier B, Tuilier M H, Lloret B, and Etourneau J 1986 *Solid State Commun.* **59** 17
[27] Vališka M, Pospíšil J, Prokleška J, Diviš M, Rudajevová A, and Sechovský V 2012 *J. Phys. Soc. Jpn.* **81** 104715
[28] Liu Z C, Li B Z, Xiao Y S, Duan Q C, Cui Y W, Mei Y X, Tao Q, Wei S L, Tan S G, Jing Q, Lu Q, Sun Y P, Liu Y Y, Fu S G, Jiang H, Ren Z, Xu Z A, Wang C, and Cao G H 2021 *Sci. China Phys. Mech. Astron.* **64** 277411
[29] Shi X B, Li J Y, Si J G, Shi L T, Liu P F, and Wang B T 2024 *Phys. Rev. B* **110** 075129
[30] Domieracki K and Kaczorowski D 2016 *Acta Phys. Pol. A* **130** 593
[31] Li H X, Lin Y Q, Yang W Z, Liu C C, Lu J Y, Li J X, Ren Z, Wang C, Jiang H, Sun Y L, and Cao G H 2025 *J. Am. Chem. Soc.* **147** 11172
[32] Felner I and Nowik I 1983 *Solid State Commun.* **47** 831
[33] Li H X, Ji L W, Lu J Y, Lin Y Q, Liu C C, Li B, Liu J, Wang C, Liu Y, Lu Y, Li Y K, Jiang H, Sun Y L, and Cao G H 2025 *J. Am. Chem. Soc.* **147** 44406
[34] Matthias B T 1955 *Phys. Rev.* **97** 74
[35] Hiebl K, Horvath C, Rogl P, and Sienko M 1983 *J. Magn. Magn. Mater.* **37** 287
[36] Guo Q, Pan B J, Yu J, Ruan B B, Chen D Y, Wang X C, Mu Q G, Chen G F, and Ren Z A 2016 *Sci. Bull.* **61** 921
[37] Matsumoto Y, Haga Y, Tateiwa N, Aoki H, Kimura N, Yamamura T, Yamamoto E, Matsuda T D, Fisk Z, and Yamagami H 2016 *J. Phys. Soc. Jpn.* **85** 104709
[38] Izumi F and Momma K 2007 *Solid State Phenom.* **130** 15
[39] Malmivirta M, Palonen H, Inkinen S, Yao L D, Tikkanen J, Huhtinen H, Jha R, Awana V P S, van Dijken S, and Paturi P 2016 *J. Phys.: Condens. Matter* **28** 175702
[40] Ren C, Wang Z S, Luo H Q, Yang H, Shan L, and Wen H H 2008 *Phys. Rev. Lett.* **101** 257006
[41] Carrington A and Manzano F 2003 *Physica C* **385** 205
[42] Wang Z C, Liu Y, Wu S Q, Shao Y T, Ren Z, and Cao G H 2019 *Phys. Rev. B* **99** 144501
[43] Johnston D C 2013 *Supercond. Sci. Technol.* **26** 115011
[44] Bardeen J, Cooper L N, and Schrieffer J R 1957 *Phys. Rev.* **108** 1175
[45] McMillan W 1968 *Phys. Rev.* **167** 331
[46] Coffey L, Levin K, and Muttalib K A 1985 *Phys. Rev. B* **32** 4382
[47] Bulaevskii L N, Dolgov O V, and Ptitsyn M O 1988 *Phys. Rev. B* **38** 11290